Enhanced specific capacity and cycling stability of flexible nanocellulose-based pseudocapacitive electrodes by controlled nanostructuring of polyaniline

Enhanced specific capacity and cycling stability of flexible nanocellulose-based pseudocapacitive electrodes by controlled nanostructuring of polyaniline

Gabriela Soukupová[a], Tereza Bautkinová[a], Petr Mazúr[a], Jarmila Vilčáková[b], Jan Prokeš[c], Marcela Dendisová[a], Miloslav Lhotka[d], Fatima Hassouna[a,*]

[a]*Faculty of Chemical Engineering, University of Chemistry and Technology, Prague, 166 28 Prague 6, Czech Republic*

[b]*Centre of Polymer Systems, Tomas Bata University in Zlín, 760 01 Zlín, Czech Republic*

[c]*Faculty of Mathematics and Physics, Charles University, 180 00 Prague 8, Czech Republic*

[d]*Faculty of Chemical Technology, University of Chemistry and Technology, Prague, 166 28 Prague 6, Czech Republic*

[*]*Corresponding author. E-mail address: fatima.hassouna@vscht.cz (F. Hassouna).*

ABSTRACT

Flexible, lightweight and electrically conductive composites based on renewable resources have recently attracted a growing interest for the development of high performance sustainable energy storage devices that can meet the needs of modern wearable and portable electronics. Herein, we developed a high performance carbon black@polyaniline ($PANI$) based flexible electrodes using a facile, low cost and environmentally friendly strategy. The strategy consisted of a co-deposition and nanostructuring of $PANI$ layer with tailored morphology on the surface of carbon black and nanofibrillated cellulose (NFC) via in situ polymerization. NFC acted as a mechanical skeleton and imparted the electrode with strength and flexibility to ensure excellent electrochemical performance. The co-doping of $PANI$ chains via a combination of a primary/secondary dopant, namely, HCl/poly(2-acrylamido-2-methyl-1-propanesulfonic acid), was used to control the morphology of $PANI$. Correlation between the textural properties of the carbon black, NFC loading, and the properties of the resulting electrodes was established. The maximum specific capacitance of 363 ± 9 F/g at the potential scan rate of 50 mV/s was exhibited by the electrode with 60% of active material loading, for which an effective growth of hierarchical nanostructures of carbon black@PANI on the surface of NFC was achieved, leading to the highest specific surface area of the composite (861 m^2/g) and a to a microporosity/mesoporosity balance. The remarkable cycling stability of the hybrid electrodes was attained as the specific capacitance retention was close to 100% with a negligible capacity decay within the tested period (over 500 cycles) regardless of the amount of the active material. This study provides an eco-friendly and cost-effective way to prepare high performance flexible electrodes for pseudocapacitors

Keywords: Polyaniline, nanofibrillated cellulose, carbon black, free-standing composite film, electrochemical properties

1. Introduction

The last decade has witnessed growing appeals for flexible, lightweight, and high capacity storage devices that can be used in portable and wearable electronics, and implantable biosensors [**1,2**]. Among the energy storage devices, supercapacitors have received much attention. Electrochemical capacitors known as supercapacitors are energy storage devices of high-power density. Flexible electrodes for supercapacitors are energy storage materials that can be operated under repeated deformation (i.e., bending) [**3**]. For this purpose, electrochemically active substances are often integrated with a flexible matrix or skeleton to manufacture flexible electrode material. Nanofibrillated cellulose (NFC) has attracted a considerable attention as a flexible matrix in the fabrication of electrodes for supercapacitors, into which the active materials are integrated. NFC is extracted from natural cellulose (e.g., wood pulp) via chemical or mechanical treatments [**4**]. It exhibits low density, high aspect ratio and high Young modulus (up to 250 GPa) [**5**]. Mechanically stable and flexible electrodes can be synthesized when NFC is interwoven [**6**]. NFC can act as a mechanical skeleton capable of a high deformation, and also as a reservoir for liquid electrolytes to facilitate ion transportation, which is responsible for the enhancement of the specific capacitance [**4,7-9**]. Conducting polymers have developed into a promising class of pseudocapacitive electrode materials for supercapacitors, owing to their relatively high theoretical capacities ($\sim$ 100 to 140 mA h/g), intrinsic electrical conductivity ($\sim$ 100 to 10,000 S/m), versatility, low environmental impact, lightweight and inexpensiveness [**10-12**]. They display higher specific capacitances than the conventional carbon-based electrodes used for supercapacitor construction [**13**]. The energy storage mechanism in pseudocapacitors is based on a faradaic process (known also as a redox process), during which a charge passes between the electrolyte and the electrode similarly to charging / discharging process of a secondary battery. Among the conducting polymers, polyaniline ($PANI$) based electrodes have enormous potential for application in pseudocapacitors. Loading of NFC with $PANI$ has been reported as a perspective way to generate flexible electrodes [**14-16**]. The pseudocapacitance of $PANI$ results from the redox process, in which doped ions are adsorbed and desorbed reversibly from macromolecular chains. However, $PANI$-based electrodes experience structural instability (chemically and mechanically) caused by the repeated volumetric swelling and shrinking of PANI during the charge/discharge process [**17-19**]. This volumetric alteration leads to structural damage of the electrode, and hence to a rapid capacitance decay of PANI [**20,21**]. According to the studies reported in the literature, most $PANI$-based electrodes retain less than 50% of their initial capacitance after about 1000 oxidation-reduction cycles [**22,23**]. Thus, cycling instability is the main hurdle of the practical use of $PANI$-based electrodes.

Recently, reported studies on hierarchical $PANI$ nanostructures turned out to be promising in overcoming this insufficient stability and enlarging the specific surface area of $PANI$-based electrodes for high-performance pseudocapacitors [**9,24**]. For instance, carbonaceous materials (e.g., graphene and carbon nanotubes) and $PANI$ nanostructures exhibited enhanced capacitance and cycling stability compared to neat $PANI$ [**13**].

Carbon blacks are the cheapest carbonaceous materials and the most used one in many types of battery and supercapacitor electrodes. Highly conductive carbon blacks (in the range 10^{-1} to 10^{2} $1/\Omega$ cm^{-1} exhibit small particle size, high porosity and a chemically clean surface (oxygen free) [**25**]. They cover a wide range of specific surface area (S_{BET}), in the range 10 to 1500 m^2/g. It is well-accepted that the surface area of carbon blacks is more accessible than other forms of high S_{BET} carbon [**25,26**]. Electrical double-layer (EDL) capacitor electrodes prepared from high S_{BET} carbon blacks exhibit high specific capacitances of up to 250 F/g, which corresponds to double-layer capacitances ranging from 10 to 16 $\mu F/cm^2$ [**25-27**]. Owing to their textural features and electrochemical performance, it would

be beneficial to employ the carbon blacks as low-cost carbon supports for nanostructuring of $PANI$ (carbon black@$-PANI$ nanosctructures) to enhance the cycling stability of $PANI$-based pseudocapacitor electrodes. However, the main challenge of this strategy is to deposit $PANI$ on the surface of carbon blacks without sacrificing the high S_{BET} provided by the latter. Yet, the step of integrating the carbon black@$PANI$ into NFC to fabricate flexible electrode is also crucial and needs to be controlled. Herein, we developed carbon black@PANI-based flexible pseudo-capacitive electrode using a facile, low cost and environmentally friendly strategy, which consisted of a co-deposition of $PANI$ layer with tailored morphology on the surface of both carbon black and NFC via in situ polymerization. The morphology of $PANI$ was controlled by the co-doping of $PANI$ chains via a combination of primary and secondary dopants. As a primary dopant, HCl, a low molecular weight inorganic dopant, was selected to yield $PANI$ with high values of electrical conductivity [**28**]. Secondary dopant, PAAMPSA, owing to its macromolecular structure induces uniform crystalline nanofibrillar morphology of $PANI$ chains and additional degree of doping [**29**]. Moreover, owing to its low glass transition temperature, PAAMPSA can act as a plasticizer for $PANI$, leading to enhanced ductility. Moreover, PAAMPSA should facilitate the formation of a thin layer-like $PANI$ on a substrate [**30**]. Correlation between the S_{BET} and the average diameter of the carbon blacks and the morphology, textural properties, electrical conductivity, mechanical and electrochemical performance of the electrodes was established. NFC acted as a mechanical skeleton and imparted the electrode with strength and flexibility to ensure promising electrochemical performance.

2. Experimental part

2.1. Materials

Nanofibrillated cellulose (NFC, 3%) was kindly donated by Weid-man. Aniline (99.5%), ammonium persulfate (APS, 98%) and 2-acryla-mido-2-methyl-1-propanesulfonic acid (AAMPSA, 99%) were supplied from Sigma-Aldrich. Sulphuric acid (H_2SO_4, 97%) and hydrochloric acid (HCl, 35%) were purchased from Penta. Carbon blacks, namely Black Pearls 2000 (BP) and Vulcan VXC72R (VC) were kindly donated by Cabot.

2.2. Materials preparation

2.2.1. Preparation of hybrid PANI-carbon black-NFC electrodes

The hybrid electrodes PANI-carbon black-NFC were prepared by in situ chemical oxidative polymerization of aniline on the surface of NFC and carbon black in the presence of HCl and AAMPSA for the dual doping [**31**]. The ratio between $PANI$, NFC and carbon black was varied while the total solid content was kept constant (750 mg in 120 ml of 1 M HCl aqueous solution). The ratio aniline: AAMPSA was also adjusted to 1:2. **Table 1** summarizes the composition of the prepared electrodes and their designation, where the ratio in w/w% of PANI-carbon black: NFC is denoted at the end of the sample name. In all experiments the ratio $PANI$: carbon black was set to 2:1 while the ratio $PANI$-carbon black: NFC was varied. The ratio of PANI to carbon black was selected based on a preliminary screening of the optimum composition at which optimal balance of mechanical, conductivity and electrochemical properties can be attained. As a reference material, $PANI-NFC$ free of carbon black was also prepared in PANI to NFC ratio of 50:50, since this composition was found to exhibit the best balance of mechanical and electrochemical properties according to our previous work [**31**].

In a typical experiment, carbon black (BP or VC) was suspended in 60 ml of 1 M HCl aqueous solution and sonicated for 10 min (PS 3000, PowerSonic). Then, a mixture of AAMPSA, NFC, aniline and 55 ml of 1 M HCl was added to the carbon black suspension and stirred at 300 rpm. The reaction system was cooled down using an ice bath for 30 min before the dropwise addition of 5 ml of APS aqueous solution (0.15 wt. %) in 1 M HCl. The suspension was left to react overnight under constant stirring at 300 rpm. The resulting product of synthesis has dark green color, indicating the formation of PANI emeraldine salt (electrically conductive form of PANI). The reaction product was filtered and washed several times. The filtered product was then redispersed in 80 ml of deionised water by sonication for 5 min (PS 3000, PowerSonic). Subsequently, the amount of slurry to cast on glass mold was calculated to gain 3 mg of active material ($PANI$ + carbon black) in 1 cm^2 of the prepared film.

2.3. Characterization methods

2.3.1. Raman spectroscopy

Dispersive Raman spectrometer with the microscope InVia Reflex was used for the chemical characterization of the electrodes. Spectra were collected using the microscope. Excitation wavelength 785 nm with laser power of 2 mW was used. 10 accumulations taking 30 s were recorded for one acquisition and final spectrum is average of 10 acquisitions.

2.3.2. X-Ray photoelectron spectroscopy

Surface chemistry of the electrode films was assessed using X-ray photoelectron spectroscopy (XPS) Omicron Nanotechnology XPS composed of a monochromatic radiation of Al lamp with excitation energy of 1486.7 eV. The software CasaXPS was used for the spectral deconvolution.

Table 1 Overview of prepared films and amounts of used components.

Sample name	Active material: NFC (w/w%)	Amount of reactants				
		Aniline (mg)	Carbon black (mg)	NFC (mg)	AAMPSA (mg)	APS (mg)
PANI-NFC [31]	50:50	300	0	300	600	750
[PANI-VC]-NFC_60:40*	60:40	300	150	300	600	750
[PANI-BP]-NFC_60:40*	60:40	300	150	300	600	750
[PANI-VC]-NFC_50:50*	50:50	250	125	375	500	625
[PANI-BP]-NFC_50:50*	50:50	250	125	375	500	625
[PANI-VC]-NFC_40:60*	40:60	200	100	450	400	500
[PANI-BP]-NFC_40:60*	40:60	200	100	450	400	500

** : Ratio $PANI$ to carbon black (BP or VC) was fixed to 2:1 while and the ratio between active material (PANI+carbon black) and NFC was varied (ratio in w/w%).*

2.3.3. Scanning electron microscopy

Bulk morphology of the electrode films was analyzed by means of scanning electron microscope (SEM) Mira 3 LMH (Tescan) under the accelerating voltage 3 kV, working distance 15 mm and beam intensity 10.

2.3.4. Transmission electron microscopy

The morphology at a nanoscale level of the carbon black powders and the electrode films were analyzed using transmission electron microscope (TEM) 100 kV, model JEM-1010 (JEOL, Ltd.) equipped with CCD camera MegaView III (Olympus Soft Imaging Systems). In short, 10 pL of suspension was deposited on a carbon-coated electron microscopic grid. Sample contrasting was performed using 1 wt.% uranyl acetate. The grid was dried and then was introduced into the electron microscope column for analysis.

2.3.5. Nitrogen physisorption

The specific surface area (S_{BET}) was measured on a 3Flex analyser (Micromeritics, Norcross) using the gas sorption technique. The samples were degassed at 373 K prior to N_2 adsorption analysis to obtain a clean surface. The adsorption isotherms were fitted using the Bru-nauer-Emmett-Teller (BET) method. The total pore volumes were measured at the relative pressure of 0.95 and the pore size distribution was determined based on density functional theory (DFT) model N2 @ 77 on Carbon Slit Pores by NLDFT. Rouquerol criterion was used to improve the validity of the calculation and to ensure the linearity of the BET plot and positive value of the constant C for calculation monolayer capacity of the BET isotherm.

2.3.6. Tensile testing

Mechanical properties of the electrode films were assessed using universal tensile testing machine Testometric (M350-5CT) with a 100 N load cell and a 0.5 mm/min strain rate. Five specimens (20×5 mm) were tested from each sample and the average value was used for the calculation.

2.3.7. Measurement of DC electrical conductivity

To measure the room temperature electrical conductivity, a four-point method in Van der Pauw contacts arrangements was used. It is based on a Keithley 6221 DC and AC Current Source, a Keithley 2001 Multimeter as a voltmeter and a Keithley 7001 Switch System equipped with a Keithley 7011-S Quad 1 × 10 Multiplexer. Electrode films were tested as prepared while the powder materials (carbon blacks) were pressed with pressure 527 MPa for 5 min to obtain small tablets for testing.

2.3.8. Electrochemical characterization

Electrochemical properties of the electrode films (circles with a 6 mm diameter) were measured using a potentiostat SP300 (Biologic) in 3-electrode arrangement in 1 mol/dm^3 H_2SO_4 electrolyte. A mercurous sulfate reference electrode (MSE) with saturated K_2SO_4 inner electrolyte (0.65 V vs. SHE) and platinum sheet counter electrode were used. Experiment consisted from cyclic voltammetry (CV) and galvanostatic charging discharging (GCD) at various constant currents. CV was performed in the potential range from -1.0 V to 0.5 V vs. MSE with the scan rate 50 mV/s. The specific capacitance was calculated in the potential range from -0.8 V to 0.2 V vs. MSE with Eq. (2) using the integration of charge (Q).

$$C = \frac{1}{Ev}\int_{E_1}^{E_2} i\,dE = \frac{1}{(E_2 - E_1)v}\int_{E_1}^{E_2} i\,dE \qquad (1)$$

In this equation, E represents the potential window, where E_2 and E_1 are its boundaries, v is a scan rate, i is a current, and dE represents changes in potential. The calculated capacitance was divided by the mass of active material in the sample or by the total mass of used composite for the purpose of comparison.

GCD was measured firstly at various constant currents (2, 5, 10 and 15 mA, corresponding to the gravimetric current densities of 4, 9, 18 and 27 A/g of $PANI$) in a potential window from -1.0 V to 0.1 V vs. MSE to determine the dependence of capacitance on current load. Afterwards, GCD at constant current 2 mA (corresponding to gravimetric current density of 4 A/g of $PANI$) was performed in the same potential window to determine the mid-term cycling stability of the prepared supercapacitor within 500 cycles.

3. Results and discussion

Thin and flexible PANI-carbon black-NFC composite films with a thickness of about 70 μm were elaborated (**Fig. 1**). Electrodes with up to 40 wt.% NFC can be rolled up due to their high flexibility thanks to the NFC. Based on the stress-strain curves (**Fig. 1**a), the flexibility and mechanical strength of the films increases with the increase of NFC loading. Indeed, all properties like the elastic modulus (**Fig. 1**b), the ultimate tensile strength (**Fig. 1**c) and the elongation at break (**Fig. 1**d) improved as the NFC loading increased. Interstingly, the tensile strength and elongation at break values of the composite films containing more than 40 wt.% NFC are comparable when taking into account the standard deviations, and drop down at the highest carbon black@PANI loading (60 wt.%). Despite the drop of the overall mechanical properties in the electrode films containing 60 wt.% carbon black@PANI, the latter remained flexible. It is worth mentioning that at carbon black@PANI loadings higher than 60 wt. %, the films become brittle, and thus unsuitable for application as electrodes.

The formation of PANI layer on the NFC and carbon black surfaces was demonstrated by Raman spectroscopy and XPS analysis.

Raman spectra of all $PANI$-based composites depicted in **Fig. 2**: exhibited the characteristic peaks of $PANI$ in the form of emeraldine salt [**32**]. This is attested by the appearance of typical peaks at 716 cm^{-1} (amine deformation in bipolarons), 810 cm^{-1} (Benzenoid ring deformation), 874 cm^{-1} (C-N-C out of plane wagging and benzene ring deformation in bipolarons and polarons), 1170 cm^{-1} (C-H bending in semiquinonoid structure), 1256 cm^{-1} (C-N benzenoid stretching), 1343 cm^{-1} ($C{\sim}N^{+\bullet}$ vibration of delocalized polaronic units) and 1520 cm^{-1} (N-H bending in semiquinonoid rings).

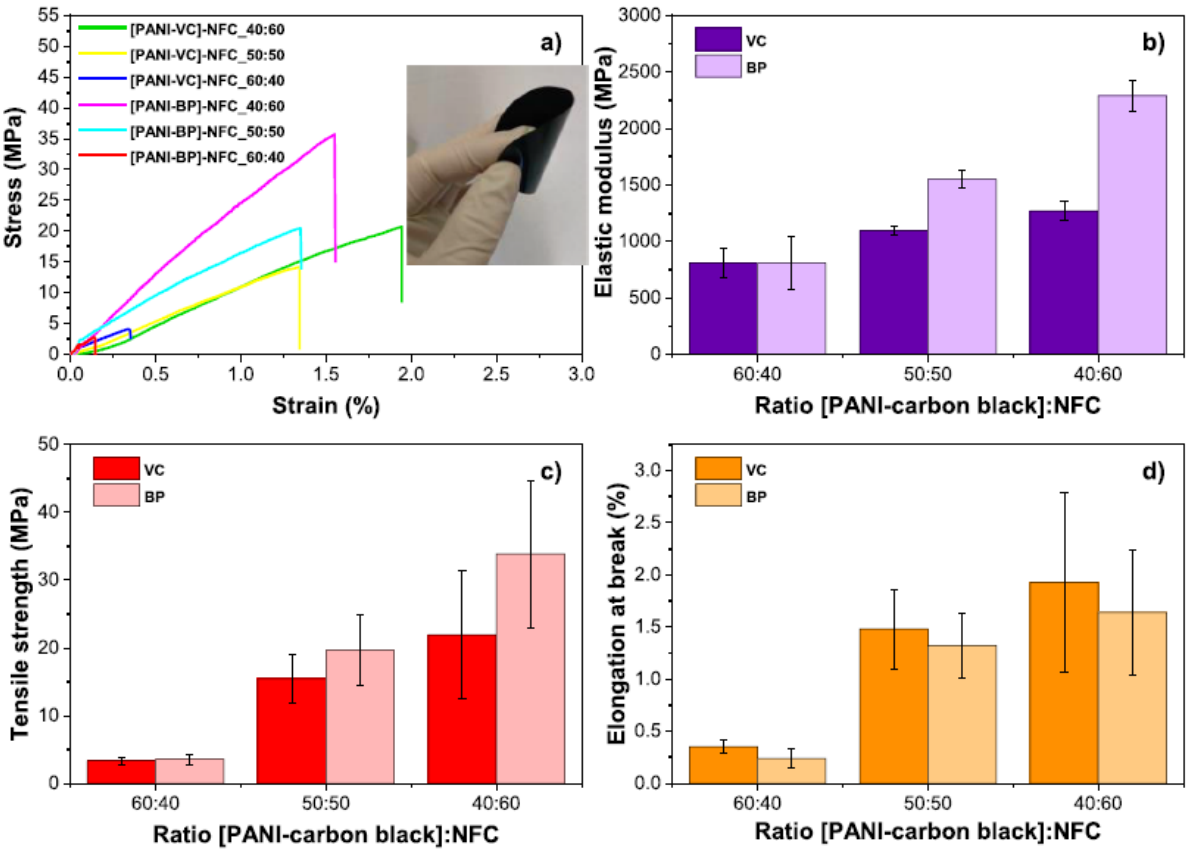

Fig. 1. Mechanical properties of $PANI$-based composites. (a) Stress-strain curves, (b) Elastic modulus, (c) Ultimate tensile strength, and (d) Elongation at break.

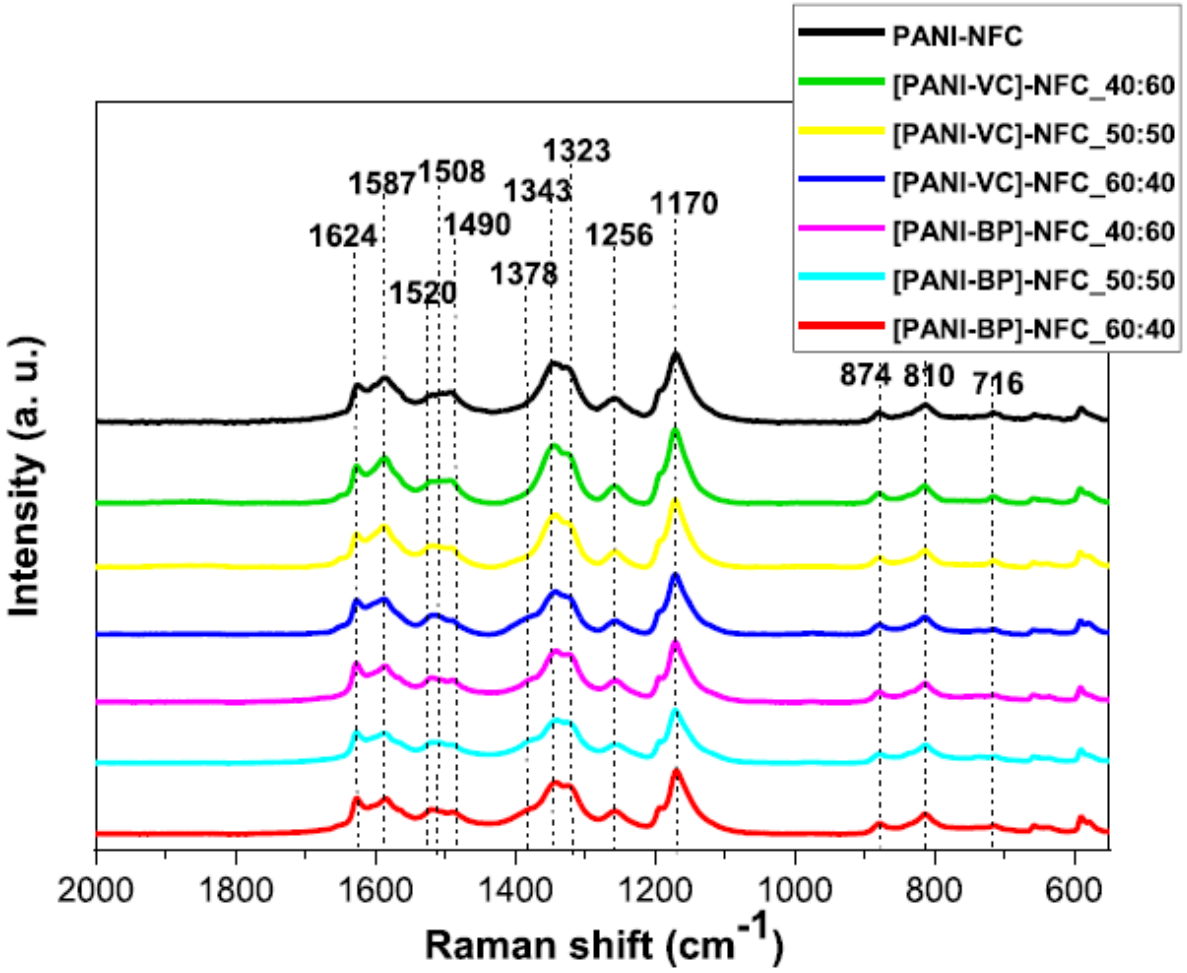

Fig. 2. Raman spectra of $PANI - NFC$ and $PANI$-carbon black-NFC electrodes.

The surface deposition of $PANI$ on carbon black and NFC was further corroborated by XPS measurements. The full survey XPS analysis of PANI-based composites are presented in Fig. S1. The proportion of the atoms being present on the surface of the composites is summarized in **Table 2**. XPS analysis show the existence of four main peaks in all PANI-based electrodes at binding energies of about 532, 400, 285 and 198 eV, attributed to oxygen (O(1s)), nitrogen (N(1s)), carbon (C(1s)) and chlorine (Cl(1s)) atoms, respectively.

The proportion of O(1s) on the surface increased while that of N(1s) dropped down with the decrease of $PANI$ loading. Higher proportion of O(1s) atoms comes from NFC, thus highlighting a lower coverage of NFC at lower PANI loading. The absence of notable increase of C(1s)) in the composites containing carbon blacks attests for their complete surface coverage with a layer of $PANI$ whatever the loading rate of the latter. The XPS spectra in the carbon region C(1s) were deconvoluted into three peaks at about 284.5 eV, 286.4 eV and 287.7 eV attributed to C—C/C = C, C—N/C—O and C=O, respectively (Fig. S2 and **Table 2**). The deconvolution shows also the increase of the amount of C—O belonging to NFC with the decrease of $PANI$ loading, which is again consistent with the lower coverage of NFC by PANI. Importantly, in order to determine the local environment of the nitrogen atoms present in PANI, XPS spectra in N(1s) region of the composites containing the highest amount of $PANI$ (good signal-to-noise ratio of nitrogen peak) were deconvoluted.

Table 2 Summary of XPS results of the $PANI$-based composites.

Sample name	Proportion of C, O and N atoms (%)				
	C	O	N	Cl	S
PANI-NFC	71.9	19.2	6.3	2.3	0.2
[PANI-VC]-NFC_60:40	67.1	23.7	6.4	2.8	
[PANI-VC]-NFC_50:50	62.8	31.8	3.9	1.5	
[PANI-VC]-NFC_40:60	57.7	39.3	2.7	0.3	
[PANI-BP]-NFC_60:40	67.6	26.6	4.4	1.4	
[PANI-BP]-NFC_50:50	61.8	34.3	3.3	0.6	
[PANI-BP]-NFC_40:60	60.3	37.0	2.0	0.7	
	Proportion of carbons (%)				
	C-N/C-O	C-C/C=C	C=O		
PANI-NFC	51.93	34.32	13.75		
[PANI-VC]-NFC_60:40	54.58	37.22	8.20		
[PANI-VC]-NFC_50:50	63.92	25.05	11.02		
[PANI-VC]-NFC_40:60	67.42	14.13	18.45		
[PANI-BP]-NFC_60:40	54.79	38.57	6.64		
[PANI-BP]-NFC_50:50	67.25	21.45	11.29		
[PANI-BP]-NFC_40:60	68.45	18.93	12.62		
	Proportion of nitrogen (%)				
	-NH-	-NH+-	-NH+=		
PANI-NFC	63.3	21.6	15.1		
[PANI-VC]-NFC_60:40	67.1	20.2	12.7		
[PANI-BP]-NFC_60:40	65.1	22.1	12.9		

As can be seen in Fig. S3 and **Table 2**, three peaks at about 399.2 eV, 400.3 eV and 401.5 eV attributed to -NH- (nitrogen atoms in secondary amine), NH^+- (delocalized polaron lattice(semiquinone segment)) and -NH^+= (localized bipolaron (pro-tonated imine)), respectively, were identified in $PANI$-NFC and [$PANI$-carbon black]-NFC_60:40 composites. Their level of protonated nitrogen moieties is about 35%. Lower signal-to-noise ratio exhibited by the other composites in N(1s) region led to decreased peak assignment. Nevertheless, based on Raman spectroscopy analysis, it is reasonable to conclude that the protonation level of PANI is likely comparable in all composites, and hence close to 35%.

The SEM and TEM micrographs of the $PANI$-based composites depicted in **Fig. 3** and **Fig. 4**, respectively, revealed morphological differences on the micro- and nano-level. While in all composites, globular-like morphology of $PANI$ on the surface of NFC fibres is revealed by SEM analysis, dissimilarities in the shape of those globules and their mean size at a nano-scale level can be associated with the presence and the type of carbon black (BP or VC). In $PANI$-NFC, NFC is covered with highly interconnected globular structures of PANI (**Figs. 3**a and **4**a). The size and morphology of the globular structures growing on NFC surface are better defined in the composites containing carbon blacks. Their size is directly proportional to that of carbon black, thus highlighting the growth of a layer of $PANI$ on the surface of the spherical carbon black nanoparticles. The mean size of the globular structures is bigger in the composites containing VC (**Figs. 3**b and **4**b, d, f) as compared to BP (**Figs. 3**c and **4**c, e, g), which is directly correlated with their respective mean diameters, i.e., 50 nm for VC and 15 nm for BP (Fig. S5). **Fig. 4** shows that the cellulosic fibrils are fully coated with globular-like nanostructures of $PANI$-carbon black in the composites [$PANI$-VC]-NFC_60:40 and [$PANI$-BP]-NFC_60:40). Below 60 wt.% of $PANI$-carbon black loading, the composites start to exhibit a heterogeneous morphology, in

which naked cellulosic fibrils can be distinguished from the coated one. These morphological features are in a good agreement with XPS results.

To track the evolution of S_{BET} and the pore size distribution of $PANI$-based composites after addition of carbon blacks, the textural properties of BP and VC powders, and $PANI$-based composites exhibiting homogeneous morphology, namely, $PANI$-NFC, [$PANI-VC$]-NFC_60:40 and [$PANI-BP$]-NFC_60:40 were evaluated by means of N_2 sorption. The surface areas were calculated using the BET equation, whereas the pore size distributions were calculated using DFT from the N_2 adsorption isotherm. N_2 sorption isotherms are shown in **Fig. 5** and the textural properties are summarized in **Table 3**.

As shown in the N_2 sorption isotherms (**Fig. 5**a and b, **Table 3**), $PANI-NFC$ showed typical type II isotherm according to the Bruner-Deming-Deming-Teller classification. $PANI-NFC$ also exhibited the lowest surface area close to 0 (S_{BET} = 4 m^2/g) and no microporosity and meso-porosity. Upon addition of carbon black, there is a change in the adsorption isotherms of $PANI$-based composites (i.e., [$PANI$-carbon black]-NFC) from type II to type IVa due to the formation of the high surface area hierarchically porous materials characterized by the presence of both micro- and mesopores (**Fig. 5**a). The latter is further supported by the pore size distribution curves (**Fig. 5**b). [PANI-BP]-NFC_60:40 exhibited the highest S_{BET} of 861 m^2/g and total pore volume (1.24 cm^3/g), which is believed to be due on one hand to the fine coating of $PANI$ on the surface of BP (S_{BET} = 1416 m^2/g), and on the other hand to the full coverage of NFC surface with carbon black@PANI.

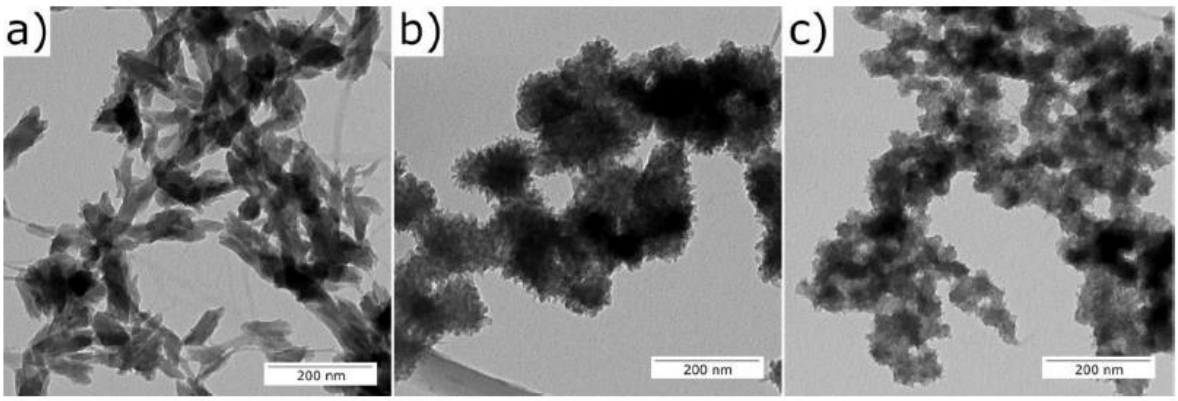

Fig. 3. TEM pictures of composites: (a) $PANI-NFC$, (b) [$PANI-VC$]-NFC_60:40, and (c) [$PANI$-BP]-NFC_60:40.

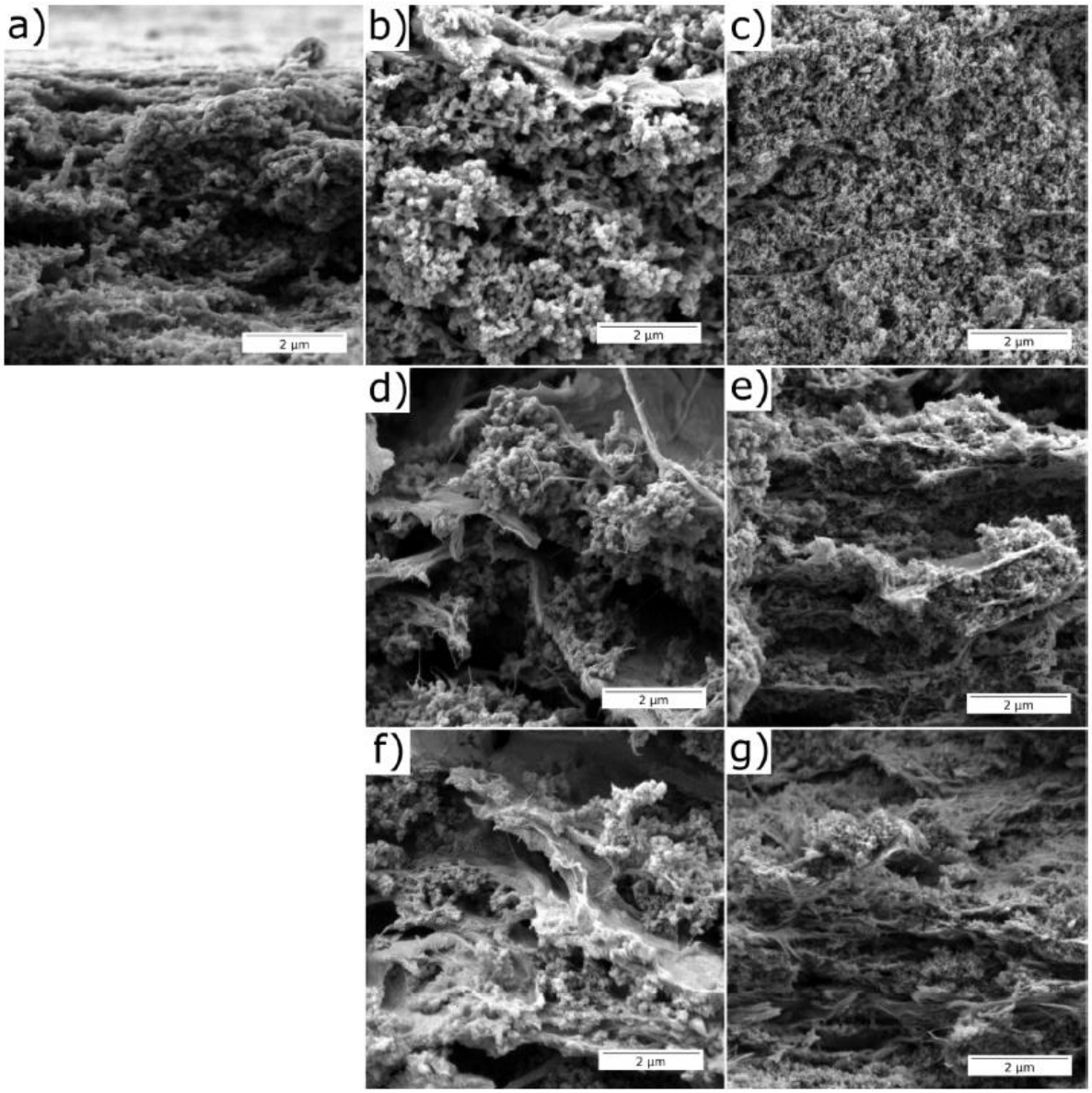

Fig. 4. SEM pictures of composites: (a) $PANI - NFC$, (b) [$PANI - VC$]-NFC_60:40, (c) [$PANI - BP$]-NFC_60:40, (d) [$PANI - VC$]-NFC_50:50, (e) [$PANI - BP$]-NFC_50:50, (f) [$PANI - VC$]-NFC_40:60, and (g) [$PANI - BP$]-NFC_40:60.

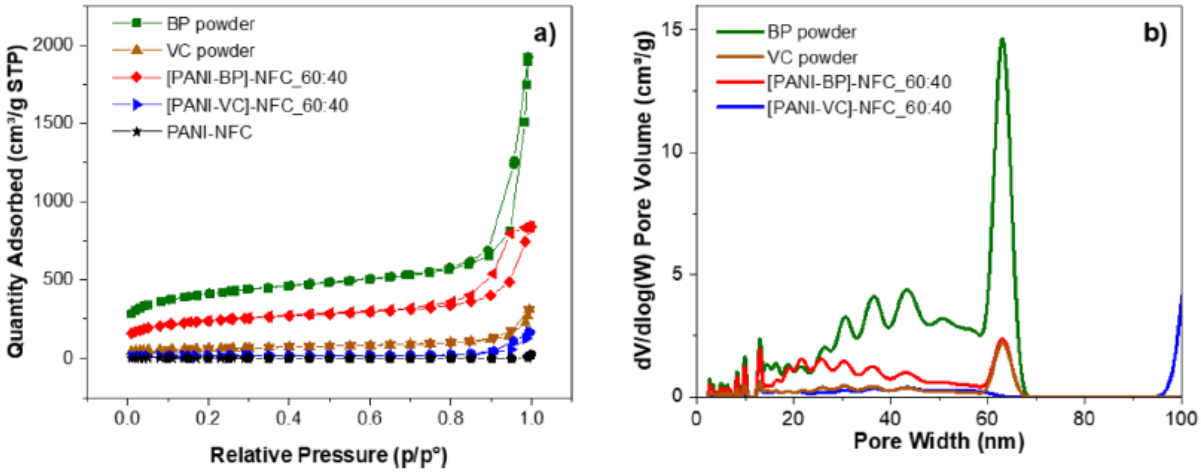

Fig. 5. Nitrogen adsorption-desorption isotherms (a), and pore size distributions (b), carbon black powders and $PANI$-based composites.

Table 3 Textural properties of the carbon black powders and $PANI$-based composites.

Material	S_{BET} [m^2/g]	$V_{micropore}$ [cm^3/g]	$V_{mesopore}$ [cm^3/g]	Isotherm type
VC powder	216±3**	0.04	0.23	IVa
BP powder	1416±22*	0.28	1.49	Ib and IVa
PANI-NFC	4±0.7	0	0	II
[PANI-VC]-NFC_60:40	62±0.3	0.01	0.15	IVa
[PANI-BP]-NFC_60:40	861±7	0.14	0.10	IVa
[PANI-VC]-NFC-50:50	24±0.4	0	0.02	IVa
[PANI-VC]-NFC-40:60	30±0.4	0	0.03	IVa
[PANI-BP]-NFC-50:50	23±0.2	0	0.08	IVa
[PANI-BP]-NFC-40:60	16±0.1	0	0.08	IVa

*: *$S_{BET} = 1500\ m^2/g$ and.*

**: *S_{BET} = 250 m^2/g according to the supplier.*

Comparatively, [$PANI - VC$]-NFC_60:40 displayed a significantly lower S_{BET} (62 m^2/g) due to lower S_{BET} of VC (S_{BET} = 216 m^2/g). Interestingly, the S_{BET} is almost four times lower in [$PANI - VC$]-NFC_60:40 than in VC while the S_{BET} of [$PANI - BP$]-NFC_60:40 is less than twice lower than BP. This trend difference in the S_{BET} between the carbon black and its corresponding $PANI$-based composite indicates the decisive role of the surface to volume ratio of the carbonaceous nanoparticles for the optimum surface coating of carbon black@$PANI$ without sacrificing the high S_{BET} provided by the latter.

Interestingly, a significant drop of the S_{BET} down to 16-30 m^2/g in all $PANI$-based composites with lower PANI-carbon black loading below 60 wt.% was observed (**Table 3**). As for $PANI - NFC$, the

composites exhibited type II isotherm (Fig. S4). The drastic textural changes observed in composites with PANI-carbon black loadings lower than 60 wt.% compared to [$PANI$-carbon black]-NFC_60:40 can be correlated with the heterogeneity of the composites, where naked cellulosic fibrils can be differentiated from the covered one, hence leading to a significant contribution of NFC to the overall textural properties.

The impact of the textural and morphological changes induced by the addition of BP and VC on the electrical and electrochemical properties of $PANI$-based composites was assessed. As can be seen in **Fig. 6**, integration of VC into PANI-NFC does not affect the electrical conductivity of the composite since both $PANI - NFC$ and [$PANI - VC$]-NFC_60:40 exhibited comparable electrical conductivity values ($\sim$ 2.5 S/cm). However, the composite containing BP exhibited higher conductivity values, e.g., 3.76 S/cm for [$PANI - BP$]-NFC_60:40.

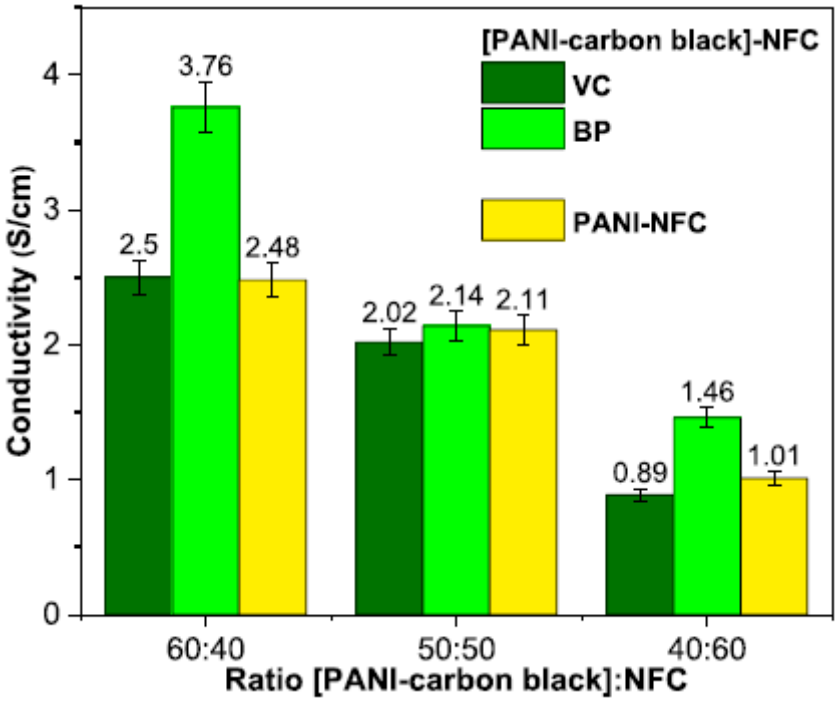

Fig. 6. Values of electrical conductivity of $PANI$-based composites.

The conductivity enhancement of [$PANI - BP$]-NFC_60:40 can be related to the effective growth of hierarchical nanostructures of carbon black@PANI on the surface of NFC whose S_{BET} of carbon black was the highest (1416 m^2/g) [**33-35**]. The electrical conductivity values of [$PANI - BP$]-NFC and [$PANI - VC$]-NFC dropped down as NFC loading increased from 40 to 60 wt.% due to the insulating features of NFC.

Fig. 7 shows the CV curves of the PANI-based composite electrodes with different ratio of [$PANI$-carbon black] to NFC in a potential window of -1 V to 0.5 V vs. MSE. CV curves of all composite electrodes show the presence of two pairs of redox peaks. They are attributed to the reversible charge-discharge behavior and pseudocapacitance features of $PANI$. The redox process in doped $PANI$ chains is due to the leucoe-meraldine-emeraldine and emeraldine-pernigraniline transitions [**36**]. As can be expected, the magnitude of the peak currents varied in the composite electrodes with various $PANI$-carbon black loadings (**Fig. 7**a and b). The magnitude of the peak current dropped down as the $PANI$-carbon black loading decreased because of the decreased content of the active material in the

electrodes. Interestingly, as can be seen in **Fig. 7**c, variations in the shape of the CV of the composites can be noticed between $PANI-NFC$, [$PANI-BP$]-NFC and [$PANI-VC$]-NFC. Unlike $PANI-NFC$ and [$PANI-VC$]-NFC, which exhibited identical CV shape, discrepancies can be noticed when compared with the CV of [$PANI-BP$]-NFC. Indeed, the latter shows clearly the effect of the EDL contribution of BP besides the contribution of PANI in the charge storage by faradic process, which is manifested by high capacitive currents in the potential region of the CV related to reduction process (-0.8 to -1.0 V vs. MSE). The positive-shift of the current peak for BP-based sample in the potential region related to oxidation process of the (0 to 0.2 V vs. MSE) is most likely attributed to increased ohmic and/or charge transfer resistance of the film. Thus, it is likely that in the case of [$PANI-VC$]-NFC, primarily $PANI$ was involved in the charge storage by its redox processes, while the contribution of the EDL capacitance of VC was rather insignificant. This discrepancy can be related to the previously mentioned difference in S_{BET} of both carbon additives.

The capacitance values of the $PANI$-based composite electrodes with different ratio of [$PANI$-carbon black] to NFC obtained from CV measurements at a scan rate of 50 mV/s in a potential window of -1 V to 0.5 V vs. MSE/50 mV/s are collected in **Fig. 8**. As can be seen in **Fig. 8**a and b, comparatively to $PANI-NFC$, [$PANI-VC$]-NFC_60:40 and [$PANI-BP$]-NFC_60:40 exhibited higher specific capacitances, with a maximum value for [$PANI-BP$]-NFC_60:40 ($\approx 145\pm4$ F/g of composite and $\approx 363\pm9$ F/g of $PANI$), which is comparable to other reported values for nanostructured $PANI$ electrodes [**31**]. The capacitance values per gram of composite (**Fig. 8**c) declined with the decrease of the amount of the active material in both [$PANI-BP$]-NFC and [$PANI-VC$]-NFC. This decline is more prominent in the composites containing VC. The capacitance values per gram of $PANI$ (**Fig. 8**d) also dropped significantly down in [$PANI-VC$]-NFC as the amount of the active material decreased while it remained almost constant at values of around 363 ± 23 and 338 ± 12 F/g for the composites [$PANI-BP$]-NFC_60:40 and [$PANI-BP$]-NFC_50:50, respectively, before a noticeable decrease was detected for [$PANI-BP$]-NFC_40:60. The contrasting electrochemical behavior between [$PANI-BP$]-NFC and [$PANI-VC$]-NFC at $PANI$-carbon black loadings lower than 60 wt.% is most likely caused by the balance among electrical conductivity, morphology and the textural properties (microporosity/mesoporosity balance and S_{BET}) [**25,26**] of the carbon black. The highest specific capacitances exhibited by [$PANI-BP$]-NFC also correlate with the dual contribution of both EDL capacitance and charge storage by faradic processes, whatever the $PANI-BP$ loading, as a result of combined positive factors. This includes an efficient nanostructuring of $PANI$ when using nano-carbonaceous fillers exhibiting high S_{BET} (i.e., BP), and also to the abundance of micropores in the latter, which plays a crucial role in the optimization of the EDL surfaces, and then strengthen the capacitance value [**37**]. Note that S_{BET} of the films does not have a significant impact on the specific capacitance values. This could be explained by the difference in the wettability of the films and the high flexibility of the gel-like nature of NFC in the presence of the electrolyte, which modifies completely the textural properties of the material in the wet medium.

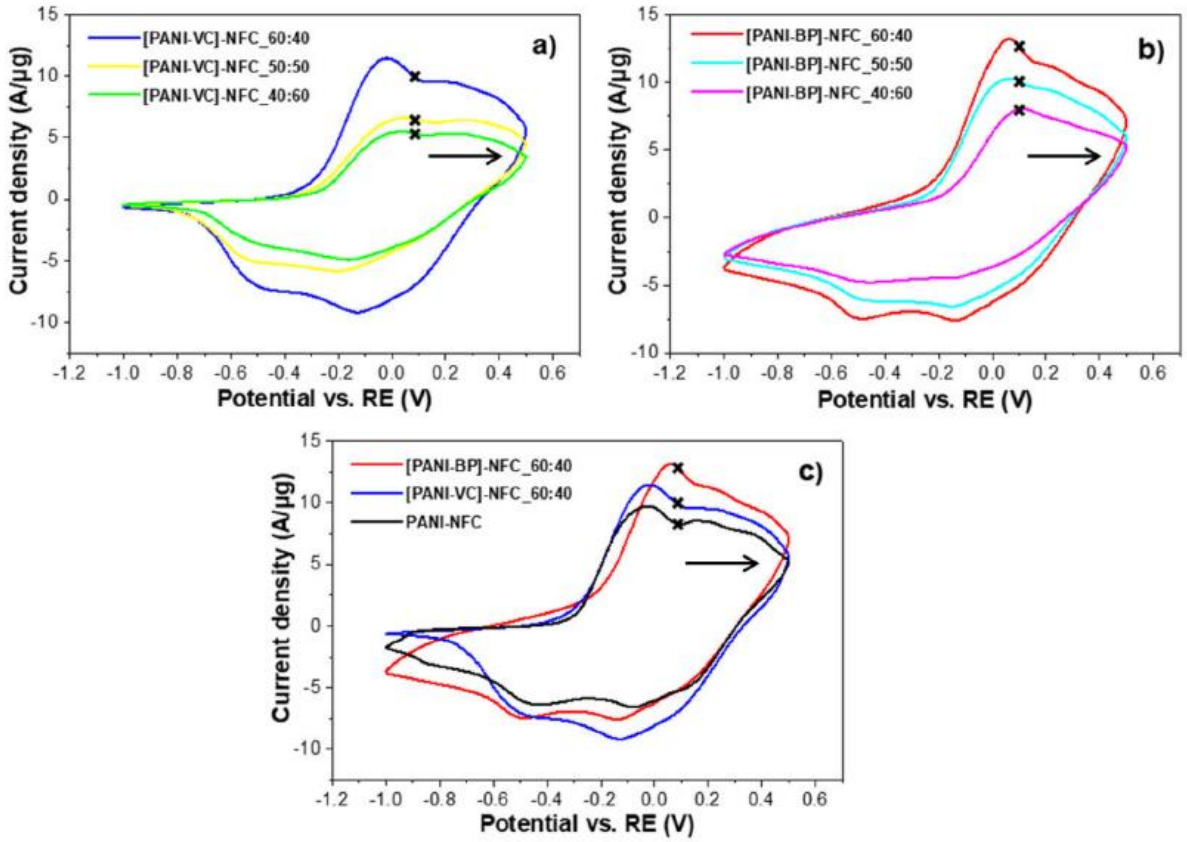

Fig. 8. Electrochemical performance of $PANI$-based composites. Specific capacitance values of $PANI-NFC$, [$PANI-VC$]-NFC_60:40 and [$PANI-BP$]-NFC_60:40 (a) per gram of composites and (b) per gram of $PANI$. Specific capacitance values of $PANI-NFC$ and $PANI$-carbon black-NFC (c) per gr of composites and (d) per gram of $PANI$.

The electrochemical performance of the films was further tested by GCD at various constant currents. The potential development within a single GCD cycle as a function of the capacity is for the individual films shown in **Fig. 9**a. In agreement with the CVs (shown on **Fig. 7**), we observed oxidation and reduction potential plateaus in the potential region from -0.6 V to -0.2 V vs. MSE corresponding to the redox transitions of $PANI$.

The rate capability of the electrodes was investigated by varying the applied current from 2 to 15 mA. **Fig. 9**b and c show the evolution of the specific capacitance as a function of the applied current within these GCD experiments. All the films show a noticeable dependence of the specific capacitance on the current load, which is reflected by the decrease of the specific capacitance with the increased applied current. This expected dependency is caused by increased ohmic and charge transfer polarization of the electrode, which decreases the capacity utilization of $PANI$ within the charge-discharge cycle [**38**]. Interestingly, the specific capacitance was found the highest for the electrode for [$PANI-BP$]-NFC_60:40 owing to the highly nanostructured $PANI$ in the presence of BP, which can create narrower and more winding transport paths for the charge carriers [**39**].

The cycling stability of the electrodes was evaluated from the GCD at constant current of 2 mA (gravimetric current density of 4 A/g of $PANI$) in the potential range — 1 V to 0.1 V vs. SHE as shown in **Fig. 9**d and e. Overall, the cycling stability over 500 cycles of the $PANI$-based electrodes was improved by the presence of both types of carbon black fillers (**Fig. 9**e).

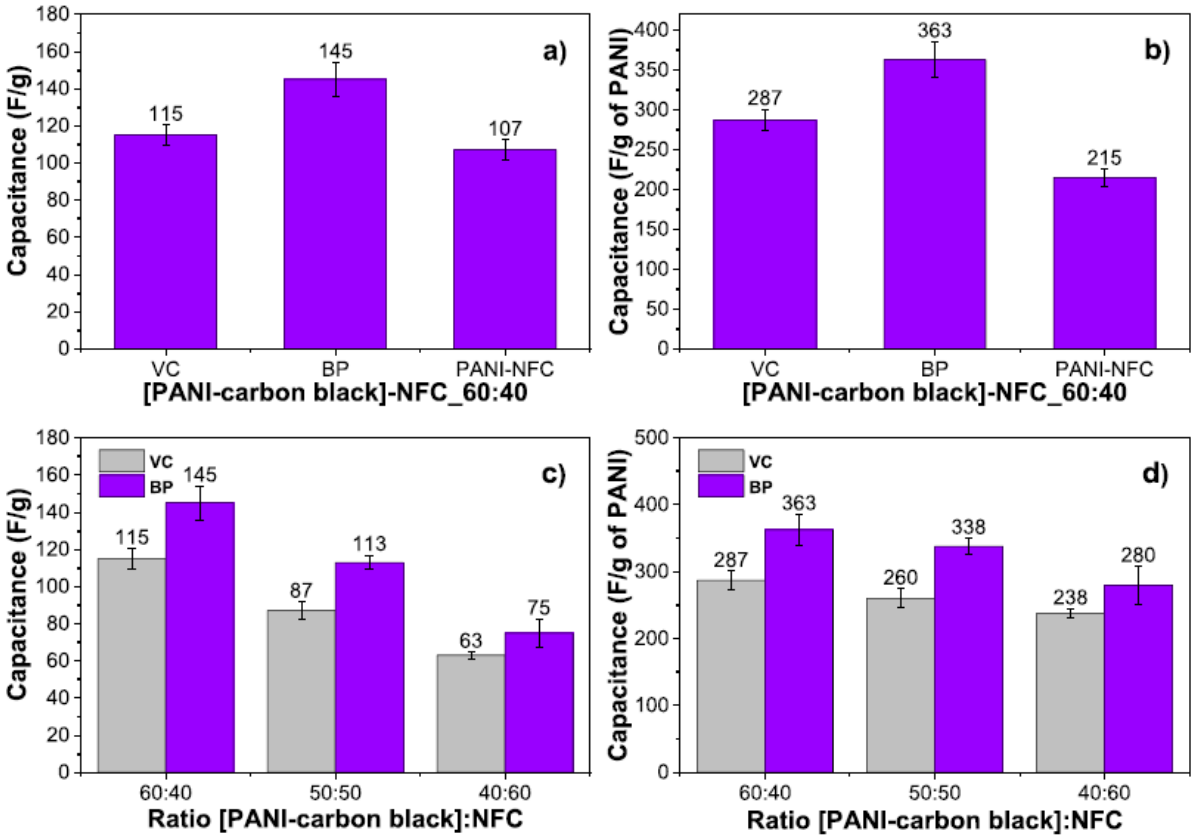

Fig. 8. Electrochemical performance of $PANI$-based composites. Specific capacitance values of $PANI-NFC$, [$PANI-VC$]-NFC_60:40 and [$PANI-BP$]-NFC_60:40 (a) per gram of composites and (b) per gram of $PANI$. Specific capacitance values of $PANI-NFC$ and $PANI$-carbon black-NFC (c) per gr of composites and (d) per gram of $PANI$.

The cycling stability of the composites containing BP and VC is remarkable as the specific capacitance retention was close to 100% with a negligible capacity decay within the tested period of 500 cycles, regardless the amount of the active material. The good stability of carbon black containing films is also evident from the comparison of potential development within GCD experiment between first and last cycle for the selected films, which is shown on **Fig. 9f**. In contrast, $PANI-NFC$ without carbon fillers, showed significantly lower capacitance retention of about 88% (**Fig. 9**e). As it has been described in the introduction, the specific capacitance decay is commonly observed for $PANI$-based pseudocapacitors due to the repeated volumetric swelling and shrinking of $PANI$ during the charge and discharge process [**11,18**]. leading to structural damage of $PANI$ [**40**]. Nanostructuring of $PANI$ using both carbon fillers, regardless of the textural properties of the latter, enhanced the cycling stability of the electrodes, which may be related to mitigation of volume changes of thin layer $PANI$ during the doping and de-doping process [**39,41**].

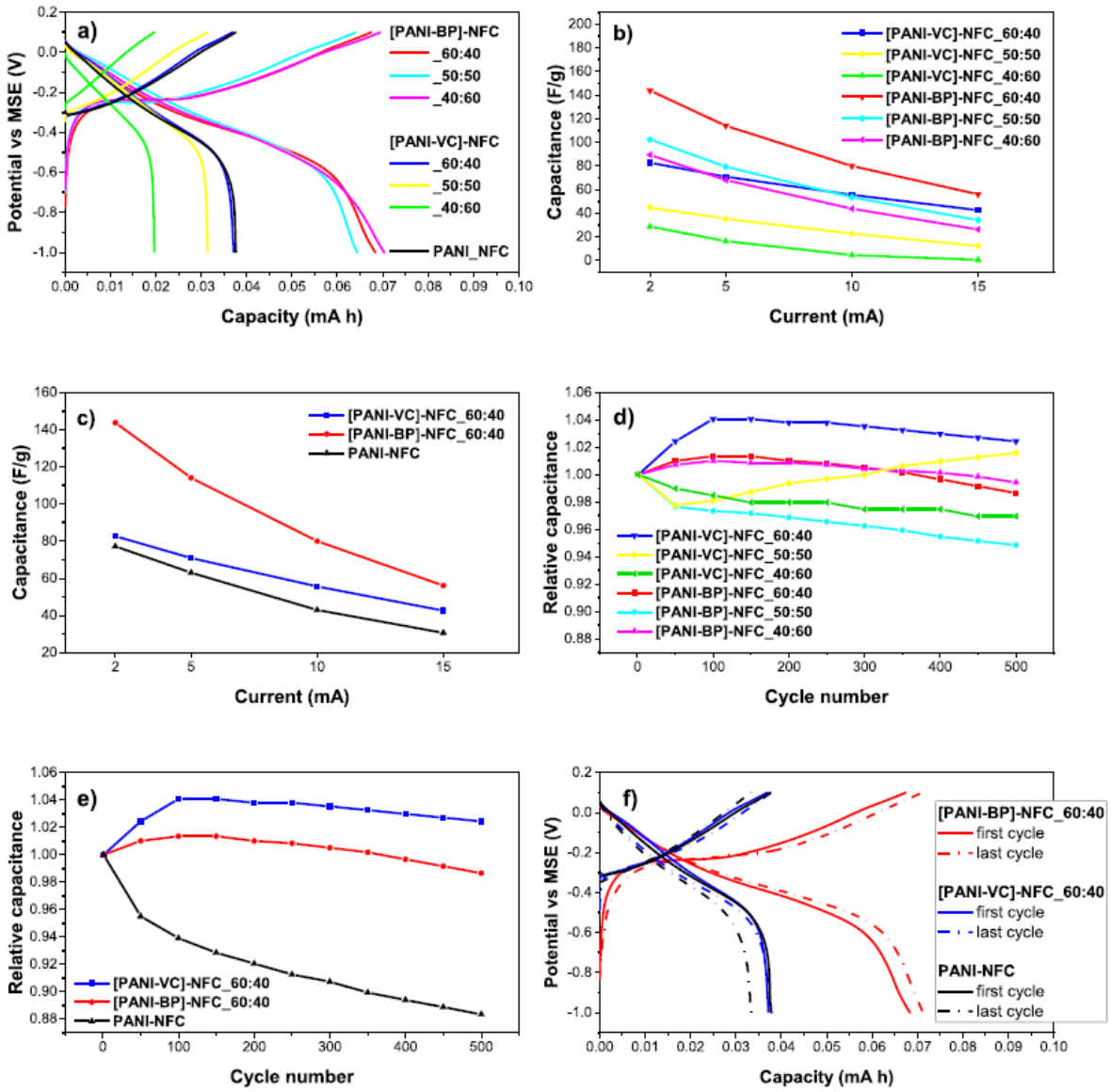

Fig. 9. Electrochemical performance of $PANI$-based composites. (a) and (b) Dependence of relative capacitance on number of cycles at constant current of 2 mA (current density of 4 A/g of $PANI$), (c) and (d) Dependence of specific capacitance on the current, and (e) and (f) Electrode potential development during charging and discharging during GCD experiment in 1 mol/dm^3 sulfuric acid at 4 A/g of $PANI$.

4. Conclusions

In summary, carbon black@PANI-based flexible pseudo-capacitor electrode using a facile, low cost and environmentally friendly strategy was developed. The strategy consisted of a co-deposition of $PANI$ layer with tailored morphology on the surface of both carbon blacks and NFC via in situ polymerization. The morphology of $PANI$ was controlled by the co-doping of $PANI$ chains via a primary (HCl)/secondary (PAAMPSA) dopants. The effect of the size and the textural properties of two types of carbon black fillers (i.e., BP and VC with Sbet of 1416 and 216 m^2/g, respectively). This study showed that the effective growth of hierarchical nanostructures of carbon black@$PANI$ on the surface of NFC (i.e., [$PANI-BP$]-NFC_60:40) leads to a remarkable enhancement of the electrical conductivity (i.e., $\sigma = 3.76$ S/cm) as well as the electrochemical performance (i.e., specific capacitance of $\approx$ 145$\pm$4 F/g of composite and $\approx$ 363 $\pm$9 F/g of $PANI$ at potential scan rate of 50 mV/s). In comparison with $PANI-NFC$ and [$PANI-VC$]-NFC, the higher specific capacitance values

exhibited by [$PANI - BP$]-NFC are correlated with the dual contribution of both EDL capacitance and charge storage by faradic processes as a result of combined positive factors. This includes an efficient nanostructuring of $PANI$ when using nano-carbonaceous fillers with high Sbet (i.e., BP), and also to the abundance of micropores in the latter, which plays a crucial role in the optimization of the electrodeelectrolyte surfaces, and then strengthen the capacitance value. Interestingly, besides the superior electrochemical performance exhibited by [$PANI - BP$]-NFC, all hybrid electrodes including [$PANI - VC$]-NFC exhibited remarkable cycling stability, with the specific capacitance retention close to 100% and a negligible capacity decay over 500 cycles. Nanostructuring of $PANI$ using both carbon fillers, regardless of the textural properties of the latter, enhanced the cycling stability of the electrodes, which may be related to mitigation of volume changes of thin layer $PANI$ during the doping and de-doping process.

References

[1] X. Wang, X. Lu, B. Liu, D. Chen, Y. Tong, G. Shen, Flexible energy-storage devices: design consideration and recent progress, Adv. Mater. (Deerfield Beach, Fla.) 26 (2014) 4763-4782.

[2] L. Li, Z. Wu, S. Yuan, X.B. Zhang, Advances and challenges for flexible energy storage and conversion devices and systems, Energy Environ. Sci. 7 (2014) 2101-2122.

[3] M. Ren, J. Di, W. Chen, Recent progress and application challenges of wearable supercapacitors,, Batter. Supercaps 4 (2021) 1279-1290.

[4] R.J. Moon, A. Martini, J. Nairn, J. Simonsen, J. Youngblood, Cellulose nanomaterials review: structure, properties and nanocomposites, Chem. Soc. Rev. 40 (2011) 3941-3994.

[5] G. Siqueira, J. Bras, A. Dufresne, Cellulosic bionanocomposites: a review of preparation, properties and applications, Polymers (Basel) 2 (2010) 728-765.

[6] X. Du, Z. Zhang, W. Liu, Y. Deng, Nanocellulose-based conductive materials and their emerging applications in energy devices - a review, Nano Energy 35 (2017) 299-320.

[7] W. Zheng, R. Lv, B. Na, H. Liu, T. Jin, D. Yuan, Nanocellulose-mediated hybrid polyaniline electrodes for high performance flexible supercapacitors, J. Mater. Chem. A 5 (2017) 12969-12976.

[8] S. Khodabakhshi, P.F. Fulvio, E. Andreoli, Carbon black reborn: structure and chemistry for renewable energy harnessing, Carbon NY 162 (2020) 604-649.

[9] C. Chen, Y. Wang, Q. Wu, Z. Wan, D. Li, Y. Jin, Highly strong and flexible composite hydrogel reinforced by aligned wood cellulose skeleton via alkali treatment for muscle-like sensors, Chem. Eng. J. 400 (2020), 125876.

[10] G.A. Snook, P. Kao, A.S. Best, Conducting-polymer-based supercapacitor devices and electrodes, J. Power Sources 196 (2011) 1-12.

[11] L. Nyholm, G. Nystrom, A. Mihranyan, M. Str0mme, Toward flexible polymer and paper-based energy storage devices, Adv. Mater. 23 (2011) 3751-3769.

[12] Y. Huang, C. Zhi, Functional flexible and wearable supercapacitors, J. Phys. D Appl. Phys. 50 (2017), 273001.

[13] T. Liu, L. Finn, M. Yu, H. Wang, T. Zhai, X. Lu, Y. Tong, Y. Li, Polyaniline and polypyrrole pseudocapacitor electrodes with excellent cycling stability, Nano Lett. 14 (2014) 2522-2527.

[14] R. Liu, L. Ma, S. Huang, J. Mei, J. Xu, G. Yuan, A flexible polyaniline/graphene/ bacterial cellulose supercapacitor electrode, New J. Chem. 41 (2017) 857-864.

[15] Q. Gong, Y. Li, X. Liu, Z. Xia, Y. Yang, A facile preparation of polyaniline/cellulose hydrogels for all-in-one flexible supercapacitor with remarkable enhanced performance, Carbohydr. Polym. 245 (2020), 116611.

[16] H. Tan, D. Xiao, R. Navik, Y. Zhao, Facile fabrication of polyaniline/pristine graphene-bacterial cellulose composites as high-performance electrodes for constructing flexible all-solid-state supercapacitors, ACS Omega 6 (2021) 11427-11435.

[17] C. Meng, C. Liu, L. Chen, C. Hu, S. Fan, Highly flexible and all-solid-state paperlike polymer supercapacitors, Nano Lett. 10 (2010) 4025-4031.

[18] H. Wang, J. Lin, Z.X. Shen, Polyaniline (PANi) based electrode materials for energy storage and conversion, J. Sci. Adv. Mater. Devices 1 (2016) 225-255.

[19] W.A. Marmisollé, M. Inés Florit, D. Posadas, Electrochemically induced ageing of polyaniline. An electrochemical impedance spectroscopy study, J. Electroanal. Chem. 673 (2012) 65-71.

[20] P. Forouzandeh, V. Kumaravel, S.C. Pillai, Electrode materials for supercapacitors: a review of recent advances, Catalysts 10 (2020) 72.

[21] J. Stejskal, P. Kratochvíl, A. Jenkins, Polyaniline: forms and formation, Collect. Czech. Chem. Commun. 60 (1995) 1747-1755.

[22] A.G. Pandolfo, A.F. Hollenkamp, Carbon properties and their role in supercapacitors, J. Power Sources 157 (2006) 11-27.

[23] F. Beck, M. Dolata, E. Grivei, N. Probst, Electrochemical supercapacitors based on industrial carbon blacks in aqueous H2SO4, J. Appl. Electrochem. 31 (2001) 845-853.

[24] R. Richner, S. Muller, A. Wokaun, Grafted and crosslinked carbon black as an electrode material for double layer capacitors, Carbon NY 40 (2002) 307-314.

[25] K. Xia, Q. Gao, J. Jiang, J. Hu, Hierarchical porous carbons with controlled micropores and mesopores for supercapacitor electrode materials, Carbon NY 46 (2008) 1718-1726.

[26] A.B. Fuertes, G. Lota, T.A. Centeno, E. Frackowiak, Templated mesoporous carbons for supercapacitor application, Electrochim. Acta 50 (2005) 2799-2805.

[27] D.W. Wang, F. Li, M. Liu, G.Q. Lu, H.M. Cheng, 3D aperiodic hierarchical porous graphitic carbon material for high-rate electrochemical capacitive energy storage, Angewandte Chemie Int. Ed. 47 (2008) 373-376.

[28] J. Stejskal, R.G. Gilbert, Polyaniline. Preparation of a conducting polymer(IUPAC Technical Report), Pure Appl. Chem. 74 (2002) 857-867.

[29] T. Bautkinová, A. Sifton, E.M. Kutorglo, M. Dendisová, D. Kopecký, P. Ulbrich, P. Mazúr, A. Laachachi, F. Hassouna, New approach for the development of reduced graphene oxide/polyaniline nanocomposites via sacrificial surfactant-stabilized reduced graphene oxide, Colloids Surf. A Physicochem. Eng. Aspects 589 (2020), 124415.

[30] S.A. Chen, H.T. Lee, Structure and properties of poly(acrylic acid)-doped polyaniline, Macromolecules 28 (1995) 2858-2866.

[31] T. Bautkinova, P. Mazúr, G. Soukupová, M. Dendisová, J. Prokeš, J. Vilčáková, D. Kopecký, M. Lhotka, P. Ulbrich, F. Hassouna, Tailor-made dual doping for morphology control of polyaniline chains in cellulose nanofiber-based flexible electrodes: electrical and electrochemical performance, J. Mater. Sci. 57 (2022) 13945-13961.

[32] M. Trchová, Z. Morávková, M. Bláha, J. Stejskal, Raman spectroscopy of polyaniline and oligoaniline thin films, Electrochim. Acta 122 (2014) 28-38.

[33] M. Cheng, Y.N. Meng, Z.X. Wei, Conducting polymer nanostructures and their derivatives for flexible supercapacitors, Isr. J. Chem. 58 (2018) 1299-1314.

[34] E.H. Jo, H.D. Jang, H. Chang, S.K. Kim, J.H. Choi, C.M. Lee, 3 D network-structured crumpled graphene/carbon nanotube/polyaniline composites for supercapacitors, ChemSusChem 10 (2017) 2210-2217.

[35] S. Dutt, P.F. Siril, Morphology controlled synthesis of polyaniline nanostructures using swollen liquid crystal templates, J. Appl. Polym. Sci. 131 (2014) 40800, **https://doi.org/10.1002/app.40800**.

[36] V. Lyutov, V. Tsakova, Polysulfonate-doped polyanilines—oxidation of ascorbic acid and dopamine in neutral solution, J. Solid State Electrochem. 24 (2020) 3113-3123.

[37] T. Lapka, D. Kopecký, P. Mazúr, J. Prokeš, P. Ulbrich, M. Dendisová, M. Sedlačík, F. Hassouna, Elaboration and properties of nanofibrillated cellulose composites with polypyrrole nanotubes or their carbonized analogs, Synth. Met. 278 (2021) 116806, **https://doi.org/10.1016/j.synthmet.2021.116806**.

[38] A. Sarkar, G. Gopal Khan, Synthesis of BiFeO3 nanoparticle anchored TiO2-BiFeO3 nano-heterostructure and exploring its different electrochemical aspects as electrode, Mater. Today Proc. 5 (2018) 10177-10184.

[39] M.A. Bavio, G.G. Acosta, T. Kessler, Polyaniline and polyaniline-carbon black nanostructures as electrochemical capacitor electrode materials, Int. J. Hydrogen Energy 39 (2014) 8582-8589.

[40] J. Deng, T. Wang, G. Jinshan, P. Liu, Electrochemical capacity fading of polyaniline electrode in supercapacitor: an XPS analysis, Progr. Nat. Sci. Mater. Int. 27 (2017) 257-260.

[41] H.R. Ghenaatian, M.F. Mousavi, M.S. Rahmanifar, High performance hybrid supercapacitor based on two nanostructured conducting polymers: self-doped polyaniline and polypyrrole nanofibers, Electrochim. Acta 78 (2012) 212-222.